Predicted Novel High-Pressure Phases of Lithium

Jian Lv, Yanchao Wang, Li Zhu, and Yanming Ma*

State Key Laboratory of Superhard Materials, Jilin University, Changchun 130012, China

(Received 2 November 2010; published 7 January 2011)

Under high pressure, ''simple'' lithium (Li) exhibits complex structural behavior, and even experiences an unusual metal-to-semiconductor transition, leading to topics of interest in the structural polymorphs of dense Li. We here report two unexpected orthorhombic high-pressure structures *Aba*2-40 (40 atoms/cell, stable at 60–80 GPa) and *Cmca*-56 (56 atoms/cell, stable at 185–269 GPa), by using a newly developed particle swarm optimization technique on crystal structure prediction. The *Aba*2-40 having complex 4- and 8-atom layers stacked along the *b* axis is a semiconductor with a pronounced band gap >0.8 eV at 70 GPa originating from the core expulsion and localization of valence electrons in the voids of a crystal. We predict that a local trigonal planar structural motif adopted by *Cmca*-56 exists in a wide pressure range of 85–434 GPa, favorable for the weak metallicity.

DOI: 10.1103/PhysRevLett.106.015503 PACS numbers: 62.50.−p, 71.30.+h, 74.25.Jb

The light alkali elements Li and sodium (Na) are often considered to be ''simple'' metals as their electronic properties are well described by the nearly free-electron model at ambient conditions. However, there is growing evidence that these materials exhibit unexpectedly complex behavior under compression [1–4]. Especially, pressure-induced metal-to-semiconductor transitions were observed in both Li [2] and Na [4]. The insulating Na has been determined to adopt the *c*-axis highly compressed double hexagonal-close-packed structure, analogous to the Ni_2In-type structure where the Na ionic cores form the Ni sublattice and the interstitially localized electron maxima occupy the In sublattice [4].

Li adopts a simple body-centered-cubic (bcc) structure at ambient condition and transforms to a complex cubic $I\bar{4}3d$ structure at 42 GPa via the intermediate face-centered-cubic (fcc) and rhombohedral $R\bar{3}m$ structures [1]. $I\bar{4}3d$ structure is stable up to ~70 GPa, above which experimental Raman [5], electrical [6–8] and x-ray diffraction [8] measurements suggest the existence of broken-symmetry phases. Recently, Matsuoka, and Shimizu [2] reported remarkably that this broken-symmetry phase is a semiconductor, where unfortunately its crystal structure remains mystery. In theory, much effort has been directed to the exploration of high-pressure structures of Li above 70 GPa [9–13]. The observed insulation seems in accordance with earlier prediction of pairing mechanism [9], which in fact is unlikely in view of the proposed energetically much preferred *Cmca*-24 (24 atoms/cell) structure by Rousseau *et al.* [10]. The *Cmca*-24 structure is a clear metal though rather weak, and thus is in apparently contrary to the observed insulation. The very recently predicted *Pbca* structure [12] is a distortion of *Cmca*-24 structure and is still a weak metal. The predicted insulating structures in this pressure regime are pointed to the *C*2 and *Aba*2-24 (24 atoms/cell) structures proposed by Yao *et al.* [13] using a combined random-searching method [14,15] and genetic algorithm technique [16]. The *C*2 structure is composed of spiral Li-Li chains, while the *Aba*2-24 structure is also a distortion of *Cmca*-24. These two structures with very small band gaps (<0.3 eV) are calculated to be stable at 74–91 GPa and above 91 GPa, respectively [13]. It is known that the crystal structure is the basis for the deep understanding of any physical properties and the insulating feature can be fundamentally revised with a different choice of structure.

Here, we have extensively explored the high-pressure phases of Li by using our newly developed particle swarm optimization (PSO) algorithm for crystal structure prediction [17]. We discovered a novel insulating structure of *Aba*2-40 stable at 60–80 GPa, containing 4- and 8-atom layers stacked along *b*- axis, which does not share any similarity to the *Cmca*-24 and its distortions. *Aba*2-40 structure is energetically superior to the *C*2 structure and has a more pronounced band gap larger than ~0.8 eV. We also targeted on the high-pressure structures in the range of 100–500 GPa, where several new structures with phase transition sequence of $Cmca-24 \rightarrow P4_2/mbc \rightarrow R\bar{3}m \rightarrow Fd\bar{3}m$ are proposed [12]. We unraveled an intriguing orthorhombic structure of *Cmca*-56 stable at 185–269 GPa, which can be viewed as an intermediate structure between *Cmca*-24 and $P4_2/mbc$.

Our approach is based on a global minimization of free energy surfaces merging *ab initio* total-energy calculations via PSO technique as implemented in CALYPSO (crystal structure AnaLYsis by particle swarm optimization) code [18]. Our method has been successful in correctly predicting structures for various systems including elements, binary and ternary compounds [17]. The underlying *ab initio* structural relaxations and electronic band-structure calculations were performed in the framework of density functional theory within the local density approximation (LDA) and all-electron projector-augmented wave (PAW) method [19,20], as implemented in the VASP

code [21]. The PAW pseudopotential with 1.2 a.u. core radius was used with 1*s* and 2*s* electrons treated as valence. The cutoff energy (1000 eV) for the expansion of the wave function into plane waves and Monkhorst-Pack [22] *k* meshes were chosen to ensure that all the enthalpy calculations are well converged to better than 1 meV/atom.

Structure predictions through the CALYPSO code with simulation sizes up to 48 atoms/cell were performed at pressure range of 0–500 GPa. All experimental and earlier theoretical structures were successfully reproduced in certain pressure ranges, validating our methodology in application to dense Li. At low pressure, simulations readily found the experimental fcc and $I\bar{4}3d$ phases at 10 and 40 GPa, respectively. At 80–120 GPa, our simulations found the *Cmca*-24 [10], *C*2 [13], *Aba*2-24 [12,13] and *Pbca* [12] structures proposed earlier. At even higher pressure, we reproduced the $P4_2/mbc$, $R\bar{3}m$ and $Fd\bar{3}m$ structures [12] at 300, 400, and 500 GPa, respectively. Besides the above known candidate structures, two new stable structures were found. At 70 and 80 GPa, simulations revealed an orthorhombic *Aba*2 structure [23] (40 atom/cell, *Aba*2-40) as depicted in Figs. 1(a) and 1(b). In this structure, Li atoms locate on five different eightfold 8*b* sites. The five crystallographically distinct Li atoms form a zigzag chain. At 70 GPa, the Li . . . Li distances are in the range of 1.61–1.82 Å, alternating along the zigzag chain. It was earlier suggested [13] that the bond alternation can be the result of Pierels distortion. All the 5-atom chains are identical, and they form a threefold structure. The *Aba*2-40 structure can also be viewed as 4- and 8-atom *a*-*c* layers stacked along the *b* axis. It has six layers: two symmetry-related 4-atom layers (shown in grey), and four symmetry-related 8-atom layers (shown in black). Upon increasing pressure to 200 GPa, an orthorhombic *Cmca* structure [23] with 56 atoms/cell (*Cmca*-56) is uncovered as shown in Fig. 1(c) and the preliminary result has been reported in Ref. [17]. This structure is in fact a threefold coordinated structure, which can be understood as alternatively stacking of the *Cmca*-24 and $P4_2/mbc$ structures. It is noteworthy that the *Cmca*-24, *Cmca*-56 and $P4_2/mbc$ structures possess similar structural features, where each Li atom and its three nearest neighbors form a trigonal plane, and these structures can be seen as two interpenetrating networks [10,12].

The enthalpies of the newly predicted stable phases, calculated at the high level of accuracy, are plotted as a function of pressure in Figs. 2(a) and 2(b) to compare with the experimental and earlier theoretical structures. The experimental $I\bar{4}3d$ structure is most stable up to around 60 GPa, beyond which our *Aba*2-40 structure becomes most favorable. Note that we do not include the zero-point energy (ZPE) corrections in the enthalpy calculations

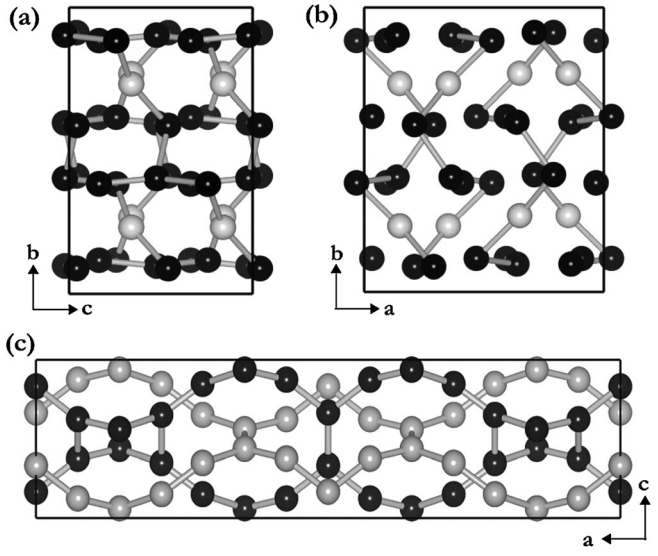

FIG. 1. (a) and (b) The predicted *Aba*2-40 structure viewed along the *a* axis and *c* axis, respectively. The grey (black) spheres represent the 4-atom (8-atom) *a*-*c* layers. (c) The predicted *Cmca*-56 structure viewed along the *b* axis. Two networks are in different shades.

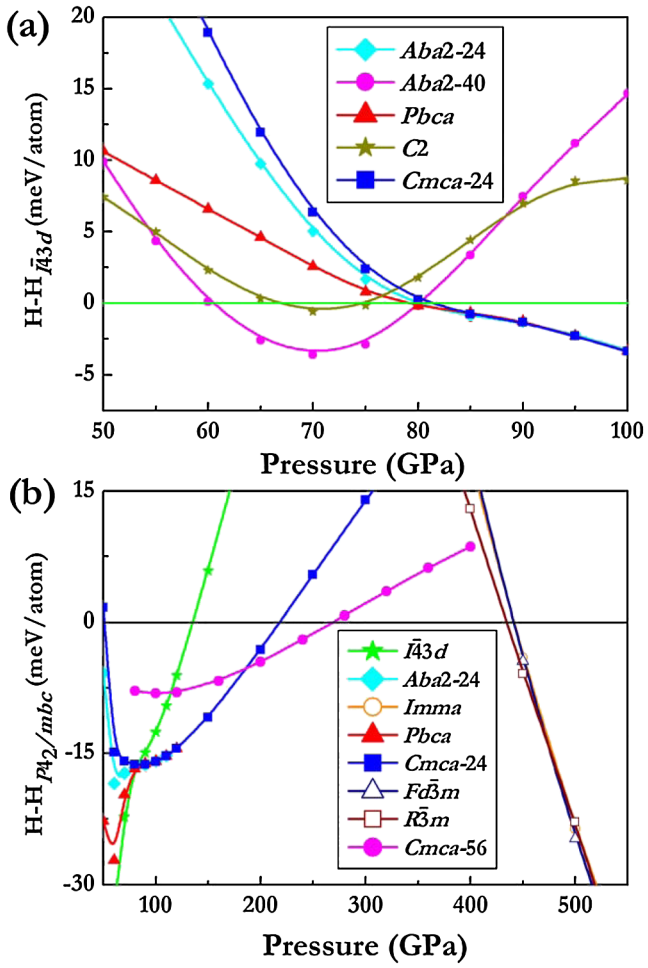

FIG. 2 (color online). (a) Calculated enthalpies per atom as functions of pressure between 50 and 100 GPa with respect to $I\bar{4}3d$ structure. (b) Calculated enthalpies per atom in the pressure range of 50–550 GPa with respect to the $P4_2/mbc$ structure.

[Figs. 2(a) and 2(b)]. Since Li has a light atomic mass, one might expect a significant ZPE contribution. Indeed, the ZP energies for $I\bar{4}3d$ and $Aba2$-40 structures at 70 GPa are estimated to have relatively large values of 86 and 87 meV/atom, respectively. However, the ZPE difference between $I\bar{4}3d$ and $Aba2$-40 is very small at $\sim$1 meV. This fact indicates that the inclusion of ZPE cannot revise the main conclusion on the structural order. The $Aba2$-40 structure has the lowest-enthalpy up to 80 GPa, where the $Pbca$ structure is calculated to be marginally most stable. In the pressure range 85–185 GPa, the enthalpies of the $Pbca$, $Aba2$-24 and $Cmca$-24 structures are almost degenerated. The emergence of several energetically degenerate and geometrically similar structures indicates the potential energy surface is overall flat with many shallow local minima and the system can be significantly frustrated by competing interactions. Since the Gibbs free energy at finite temperature is much smoother than the potential energy surface at $T = 0$, disordered structures might be stabilized in this pressure regime. Beyond the stable pressure field (> 185 GPa) for these nearly degenerated structures, the predicted $Cmca$-56 structure is found to be most energetically favorable up to 269 GPa. Our phonon calculations have verified that both $Aba2$-40 and $Cmca$-56 structures are dynamically stable by evidence of the absence of any imaginary frequency in the whole Brillouin zone.

Under compression, Li exhibits increasingly shorter interatomic distances. The nearest Li-Li distance is 1.61 Å for $Aba2$-40 structure at 70 GPa. Given that the ionic radius of Li^{1+} is 0.76 Å and the 2s-orbital radius is 1.586 Å, we deduce that the core-valance overlap is large and core exclusion already plays a significant role to the valence electrons at the stable field of the $Aba2$-40 phase. This core exclusion can induce many interesting physical effects that departed notably from the NFE behaviors, such as interstitial electronic localization and the metal-to-semiconductor transition [4,24]. Indeed, the $Aba2$-40 structure develops a band gap. As shown in Fig. 3(a), the calculated band structure and partial electronic density of states (DOS) at 70 GPa show that the density functional band gap is $\sim$0.8 eV (it should be much larger as DFT calculation underestimates band gap significantly) and a pronounced p angular momentum character is developed bellow Fermi level. At this pressure, the occupied valence bandwidth is about 31% of its free-electron value and continuously decreases as pressure is increased. This indicates the increased localization with compression. Similar effect, that is first proposed by Neaton and Ashcroft [9], has been interpreted as results of Peierls distortion and core exclusion [12,13,25,26]. The bandwidth decrease is closely correlated with the development of the p-character bonding, which lowers the band-structure energy and offsets the energy penalty by the Peierls distortion. This conclusion is further substantiated

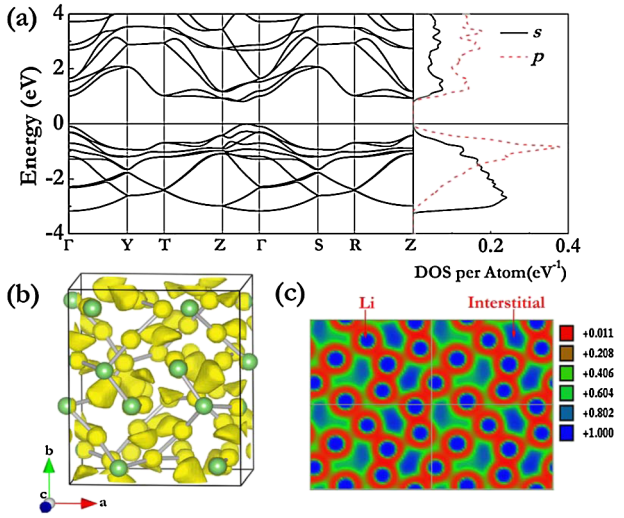

FIG. 3 (color online). (a) Band structure (left panel) and partial electronic DOS (right panel) of the $Aba2$-40 structure at 70 GPa. The Fermi energy (E_F) was set to zero. (b) Isosurface of ELF for the corresponding structure with the value of 0.85. (c) ELF plots in (010) section through the 8-atom layer.

by the electron localization function (ELF) shown in Figs. 3(b) and 3(c), where the calculated ELF with an isosurface ELF value of 0.85 indicates a substantial accumulation of electronic charge density within the voids of the crystal. It is noteworthy that the band gap in the $Aba2$-40 structure increases up to $\sim$1.5 eV at 150 GPa originated from the more localized electrons in the voids of crystal, similar to that in transparent Na [4].

Beyond the $Aba2$-40 structure, as the localization energy cost becomes larger, Li shows several other phase transitions. Because of the common structural features, the $Cmca$-24, $Cmca$-56 and $P4_2/mbc$ structures share similar electronic properties. The DOSs dip [Fig. 4(b)] around the E_F and the relative bandwidths are 28% ($Cmca$-24 at 90 GPa), 21% ($Cmca$-56 at 200 GPa), 24% ($P4_2/mbc$ at 400 GPa) of their respective free-electron values. As shown in Fig. 4(a), the valence bands of the $Cmca$-56 structure are flat with only a small amount of band overlap. As a

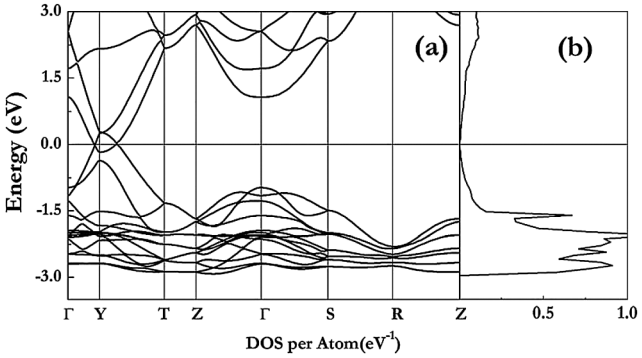

FIG. 4. Calculated electronic band structure (a) and DOS (b) of the $Cmca$-56 structure at 200 GPa.

consequence of the nearly zero-gap semiconducting behavior, compressed Li should be strongly absorptive in the visible [27]. At even higher pressure, the DOSs of the $R\bar{3}m$ (stable at 434–475 GPa) and $Fd\bar{3}m$ (stable above 475 GPa) phases still exhibit minimum at E_F and the weak metallic behavior persists.

In summary, using our newly developed PSO technique on crystal structure prediction, we report two likely candidates for the high-pressure phases of Li, *Aba*2-40 and *Cmca*-56, which are stable in the pressure ranges of 60–80 GPa and 185–269 GPa, respectively. Our calculations reveal that an insulating electronic state emerges in the *Aba*2-40 phase because core exclusion and the localization of valence electrons in the voids of crystal. Here, compression causes the $2p$ bands to rapidly drop in energy relative to the $2s$ bands, resulting in the increased transformation from s to p electrons. We found that the local trigonal planar structural motif of Li exists in a wide pressure range of 85–434 GPa. As a consequence, all post-*Aba*2-40 structures of dense Li are weak metals. The present results inevitably stimulate future experimental and theoretical study of Li at high pressure.

The authors acknowledge funding from the National Natural Science Foundation of China under Grant Nos. 10874054, 91022029, and 11025418, and the China 973 Program under Grant No. 2011CB808200. Part of the calculations were performed in the High Performance Computing Center (HPCC) of Jilin University.

*mym@jlu.edu.cn

[1] M. Hanfland *et al.*, Nature (London) **408**, 174 (2000).
[2] T. Matsuoka and K. Shimizu, Nature (London) **458**, 186 (2009).
[3] E. Gregoryanz *et al.*, Science **320**, 1054 (2008).
[4] Y. Ma *et al.*, Nature (London) **458**, 182 (2009).
[5] A. F. Goncharov *et al.*, Phys. Rev. B **71**, 184114 (2005).
[6] V. V. Struzhkin *et al.*, Science **298**, 1213 (2002).
[7] S. Deemyad and J. S. Schilling, Phys. Rev. Lett. **91**, 167001 (2003).
[8] T. Matsuoka *et al.*, J. Phys. Conf. Ser. **121**, 052003 (2008).
[9] J. B. Neaton and N. W. Ashcroft, Nature (London) **400**, 141 (1999).
[10] R. Rousseau *et al.*, Chem. Phys. Chem. **6**, 1703 (2005).
[11] Y. Ma, A. R. Oganov, and Y. Xie, Phys. Rev. B **78**, 014102 (2008).
[12] C. J. Pickard and R. J. Needs, Phys. Rev. Lett. **102**, 146401 (2009).
[13] Y. Yao, J. S. Tse, and D. D. Klug, Phys. Rev. Lett. **102**, 115503 (2009).
[14] C. J. Pickard and R. J. Needs, Phys. Rev. Lett. **97**, 045504 (2006).
[15] C. J. Pickard and R. J. Needs, Nature Mater. **9**, 624 (2010).
[16] Y. Yao, J. S. Tse, and K. Tanaka, Phys. Rev. B **77**, 052103 (2008).
[17] Y. Wang *et al.*, Phys. Rev. B **82**, 094116 (2010).
[18] Yanming Ma, Yanchao Wang, Jian Lv, and Li Zhu, http://nlshm-lab.jlu.edu.cn/~calypso.html.
[19] P. E. Blöchl, Phys. Rev. B **50**, 17 953 (1994).
[20] G. Kresse, and D. Joubert, Phys. Rev. B **59**, 1758 (1999).
[21] G. Kresse and J. Furthmüller, Phys. Rev. B **54**, 11 169 (1996).
[22] H. J. Monkhorst and J. D. Pack, Phys. Rev. B **13**, 5188 (1976).
[23] See supplementary material at http://link.aps.org/supplemental/10.1103/PhysRevLett.106.015503 for detailed crystallographic information and CONTCAR files for our proposed *Aba*2-40 and *Cmca*-56 structures and earlier theoretical structures.
[24] B. Rousseau and N. W. Ashcroft, Phys. Rev. Lett. **101**, 046407 (2008).
[25] I. Tamblyn, J.-Y. Raty, and S. A. Bonev, Phys. Rev. Lett. **101**, 075703 (2008).
[26] J. Y. Raty, E. Schwegler, and S. A. Bonev, Nature (London) **449**, 448 (2007).
[27] J. B. Neaton and N. W. Ashcroft, Phys. Rev. Lett. **86**, 2830 (2001).